applied sciences

MDPI

Article

Effect of Ventilation Ducts on Coupled Heat and Moisture Transfer in Pilot Silo Wheat Bulks with Non-Uniform Porosity

Huichen Shi [1], Gang Zhang [1], Zhipeng Yao [1], Deqian Zheng [2,3,4,*], Chaosai Liu [2,3,4] and Sikang Yuan [2]

[1] Wuxi COFCO Engineering & Technology Co., Ltd., Wuxi 214000, China
[2] College of Civil Engineering, Henan University of Technology, No. 100, Lianhua Road, Zhengzhou 450001, China
[3] Henan Key Laboratory of Grain Storage Facility and Safety, Zhengzhou 450001, China
[4] Henan International Joint Laboratory of Modern Green Ecological Storage System, Zhengzhou 450001, China
* Correspondence: deqianzheng@haut.edu.cn

Abstract

Appropriate ventilation strategies are beneficial for preventing grain deterioration and losses during storage, thereby ensuring grain quality and safety. Using established porous media transport equations, the Ergun equation, and a thin-layer drying model, a coupled heat and moisture transfer framework accounting for non-uniform porosity was implemented and validated for a pilot-scale wheat silo. The engineering comparison examined four, six, and eight vertical branch ducts at a central duct height of 0.94 times the grain filling height, and central duct heights of 0.47 (0.47H), 0.94 (0.94H), and 1.07 (1.07H) times the grain filling height with four branch ducts. At a fixed total inlet mass flow rate of 0.51 kg/s, four branch ducts produced slightly faster initial cooling, while differences among the branch duct configurations diminished during approximately 40–88 h. Central duct height affected the location and extent of residual high-temperature zones, whose area ratios were described by case-specific exponential fits over the simulated ventilation interval. Among the three central duct heights examined, 1.07H produced the smallest high-temperature-zone area ratio at 88 h, whereas 0.94H produced the lowest predicted final moisture content. In the pilot silo and operating conditions of this study, the central air collecting duct positioned near or above the grain surface is beneficial for regulating the ventilation performance of the grain bulk.

Keywords: wheat; pilot silo; numerical simulation; porosity; heat and moisture transfer

Check for updates

Academic Editors: Abel Rodrigues and Marco Bietresato

Received: 4 August 2026
Revised: 17 November 2026
Accepted: 21 November 2026
Published: 24 November 2026

Copyright: © 2026 by the authors. Licensee MDPI, Basel, Switzerland. This article is an open access article distributed under the terms and conditions of the Creative Commons Attribution (CC BY) license.

1. Introduction

China's wheat production has exceeded 130 million tons for ten consecutive years [1]. After harvest, large quantities of wheat are stored in warehouses to balance seasonal production and demand, while also mitigating the impacts of natural disasters and fluctuations in market grain prices, thereby ensuring food supply security [2]. However, the processes of grain breakage and automatic grading during loading [3], together with uneven compression of the grain bulk caused by its own weight over long-term storage, lead to a non-uniform porosity distribution in the vertical direction [4], which alters the efficiency of heat and moisture transfer. The resultant accumulation of heat and moisture readily promotes mold growth and insect infestation [5], necessitating timely control measures such as ventilation [6].

The porosity within a grain bulk is a critical parameter influencing heat and moisture transfer [7,8]. Gao et al. [9] investigated the bulk density distribution of wheat in silos using

the finite element method and a modified Cam–Clay model, revealing that grain porosity varies non-uniformly along the silo radius. Moya et al. [10] conducted compression experiments on wheat samples stored in silos and developed a functional relationship between volumetric porosity and applied pressure. During aeration, variations in porosity among particle assemblies affect the airflow resistance through the interparticle voids, thereby influencing aeration efficiency [11]. Khatchatorian and Savicki [12] incorporated porosity distribution in grain bulks into a mathematical model simulating airflow patterns during aeration. They found that assuming a simple uniform porosity distribution may lead to inaccurate predictions of the physical parameters involved in aeration or drying processes. Jian et al. [13] numerically found that the airflow resistance coefficient increases with decreasing porosity and is also affected by particle size and shape. To achieve uniform airflow distribution and minimize ventilation dead zones during grain silo aeration and drying, Nwaizu and Zhang [14] investigated the effects of porosity on internal airflow in grain bulks and developed a predictive aeration system featuring a ventilated floor and horizontal airflow design. In our previous work, we explored the effects of ventilation cage height and supply air temperature on drying performance [15]. Recently, Yan et al. [16] proposed a dual-inlet hexagonal perforated duct system placed at the bottom of the grain bulk to improve ventilation uniformity. These studies provide the modeling basis for investigating airflow resistance and ventilation layouts. For the pilot configuration considered here, a further engineering question is how changing the number of wall-mounted vertical branch ducts and the relative height of a central air collecting duct redistributes airflow, residual warm zones, and moisture loss under the same total inlet flow. Comparing cooling and moisture responses together is necessary because a configuration favorable for one response may not be favorable for the other.

This study applies established porous media transport equations, the Ergun resistance correlation, and a thin-layer drying model to a pilot-scale wheat silo with non-uniform porosity. The contribution lies in the engineering comparison of the investigated radial ventilation configurations, rather than in a new governing equation or drying model. At a fixed total inlet mass flow rate, the comparisons show how branch duct number and central-duct height alter early cooling, residual high-temperature zones near the duct end, and predicted moisture loss. The high-temperature-zone area ratio is fitted as a function of ventilation time over the simulated interval, providing a case-specific measure of cooling progress. These results identify trade-offs among the tested configurations and provide a basis for further evaluation of radial ventilation designs under other silo geometries and operating conditions.

2. Ventilation System and Methods

2.1. Fluid Transport Equations

The rate of mass accumulation within a differential element of the grain bulk is equal to the net mass flow rate entering the element over the same time interval. Accordingly, the continuity equation for fluid transport within the grain bulk can be expressed as follows [17]:

$$\frac{\partial(\varepsilon\rho_a)}{\partial t} + \nabla\cdot(\varepsilon\rho_a\vec{v}) = 0 \quad (1)$$

where ε is the porosity; ρ_a is the density of air; t is the time; $\vec{v}$ is the vector velocity of air; and ∇ is the divergence operator.

The moisture transfer equation was expressed as follows [18]:

$$\frac{\partial(\varepsilon\rho_a w)}{\partial t} + \nabla\cdot(\varepsilon\rho_a\vec{v}w) = \nabla\cdot(\varepsilon\rho_a D_{eff}\nabla w) + S_w \quad (2)$$

where w is the absolute moisture content in the air between kernels; D_{eff} is the effective diffusion coefficient of water vapor; S_w represents the volumetric moisture source/sink term

due to adsorption or desorption by the wheat kernels, i.e., the mass of water exchanged between the grain phase and the interstitial air per unit bulk volume per unit time. This source term is given by Equation (3):

$$S_w = (1-\varepsilon)\rho_t \frac{\partial W}{\partial t} \tag{3}$$

Wheat bulk drying involves coupled heat and moisture transfer. A modified dual-parameter thin-layer drying model was used to investigate wheat bulk drying under mechanical ventilation, expressed as follows [15]:

$$\frac{\partial W}{\partial t} = -0.784kt^{-0.216}[W - (0.129 - 6.46 \times 10^{-4}T)(\frac{r}{1-r})^{0.3397}] \tag{4}$$

where k is the empirical coefficients of the grain drying model, $k = 2.8 \times 10^{-3} \times e^{0.059T} \times r^{-0.139} \times v^{0.025}$; r is the relative humidity of dry air.

Here, W is the moisture of the wheat bulk, and ρ_t is the dry basis density of the wheat kernels.

The momentum conservation equation is expressed as follows [8]:

$$\frac{\partial(\varepsilon\rho_a\vec{v})}{\partial t} + \nabla\cdot(\varepsilon\rho_a\vec{v}\vec{v}) = -\varepsilon\nabla p + \nabla\cdot(\varepsilon\mu\nabla\vec{v}) + S_i \tag{5}$$

where ∇p is the pressure gradient; μ is the air viscosity; and S_i is the momentum source term representing the flow resistance exerted by the porous wheat bulk on the interstitial air, which can be expressed as follows:

$$S_i = -(\frac{\mu}{\alpha}\vec{v} + \frac{C_2\rho_a}{2}|\vec{v}|\vec{v}) \tag{6}$$

where a is the permeability of the wheat bulk and C_2 is the inertial drag coefficient. Both coefficients come from the Ergun equation [19], which expresses the pressure loss of a fluid moving through a packed bed as the sum of a viscous term that is linear in the velocity and an inertial term that is quadratic in it. The same two-coefficient form has been used for stored grain bulks by Eisfeld and Schnitzlein [17] and Thorpe [18]. They are written as follows:

$$\frac{1}{\alpha} = \frac{150(1-\varepsilon)^2}{d_p^2\varepsilon^3} \tag{7}$$

$$C_2 = \frac{1.75(1-\varepsilon)}{d_p\varepsilon} \tag{8}$$

In Equations (7) and (8), d is the equivalent diameter of the wheat kernels and ε is the porosity of the bulk. The first equation accounts for the viscous shear at the kernel surfaces, the second for the inertial loss caused by the repeated acceleration and deceleration of the air as it passes through the irregular voids. Both follow from the Ergun correlation [19], which was fitted to measurements on packed beds and is widely used for granular agricultural materials.

Due to the small grain size, low gap velocity, large specific surface area, and short thermal equilibrium time of wheat, it is assumed that the grain temperature is equal to the air temperature between the pores. The energy transfer equation based on the local equilibrium heat model of porous media as expressed as follows [18]:

$$\frac{\partial(\varepsilon\rho_a C_{pa}T_a + (1-\varepsilon)\rho_g C_{pg}T_a)}{\partial t} + \nabla\cdot(\varepsilon\rho_a\vec{v}C_{pa}T_a) = \nabla\cdot(\varepsilon k_{eff}\nabla T_a) + S_h \tag{9}$$

where ρ_g is the volume density of the grain bulks; T_a is temperature; k_{eff} is the effective thermal conductivity of the grain bulk; S_h is the energy source term for the grain bulk domain, which can be expressed as follows:

$$S_h = (1-\varepsilon)\rho_t \frac{\partial W}{\partial t} h_v \tag{10}$$

where h_v is the latent heat of evaporation of water. The computational parameters are shown in Table 1.

Table 1. Parameters related to the ventilation process.

Material	Property	Value
Air [15]	Air density (ρ_a)	1.205 kg/m^3
	Air viscosity (μ)	1.79×10^{-5} Pa·s
	Air thermal conductivity (k_a)	0.025 W/(m·°C)
	Specific heat capacities of water	1850 J/(kg·°C)
	Rate coefficient for moisture exchange between air and maize kernels (D_v)	2000exp $(-5094/T)$
Wheat bulk	Moisture content (M)	12.5%
	Density of the grain bulks) (ρ_g)	800 kg/m^3
	Moisture content (dry basis) (W)	M/(1 − M) × 100%
	Dry basis density of the wheat kernels (ρ_t)	1251.6 kg/m^3
	Average maize kernel diameter (d)	0.004 m
	Wheat thermal conductivity (k_s)	$0.1296 + W$
	Effective thermal conductivity (k_{eff})	$\varepsilon \cdot k_a + (1 - \varepsilon) \cdot k_s$
	Porosity (ε)	Equation (11)
	Specific heat (C_{pa})	$C_g = 1114.79 + 9.13T + 9.25 \times 10^{-2} + (33.71 - 2.88 \times 10^{-3}T + 3.35 \times 10^{-4})W$
	Effective diffusion coefficient of water vapor (D_{eff})	$0.233D_v$
	Temperature (T)	Based on measurement results

2.2. Materials and Ventilation System

The material used in the experiment is wheat. The wheat bulk density was 800 kg/m^3, and the initial dry basis moisture content was 12.5%. Figure 1 shows the pilot silo test apparatus. The silo has a diameter of 1.5 m and a height of 3 m, with a conical roof of 0.8 m in height at the top. An air outlet is arranged at approximately half the height of the cone. Branch air ducts are installed at the bottom of the silo. The airflow supplied by a centrifugal fan passes sequentially through the bottom air inlet and the branch ducts, and then enters four vertical branch air ducts, which are set at equal intervals on the inner wall of the silo and have a height of 2.2 m, a diameter of 0.2 m, and a diameter of 2 mm. A total of 12 temperature measuring points are placed inside the grain bulk, and the spatial positions of the temperature measurement points are shown in Figure 1. The 12 temperature measurement points are divided into four layers at heights of 0.5, 0.9, 1.3, and 1.7 m above the bottom of the grain pile, with three points per layer. The radial distances between the three points and the center of the silo are 0.15, 0.35, and 0.55 m. One temperature sensor and one humidity sensor are, respectively, installed outside the silo to monitor the temperature and humidity of the supply air.

2.3. Initial Conditions of Wheat Bulk

Prior to ventilation, the wheat had been stored during the hot summer, resulting in an uneven temperature distribution within the grain bulk. The initial temperature field for the numerical simulation was determined based on the mean temperature of each layer measured in the experiment (Figure 2a). Specifically, the initial temperatures were 33.7 °C for the height range of 0.5~0.9 m, 34 °C for 0.9~1.3 m, 28.4 °C for 1.3~1.7 m, and 25 °C for heights above 1.7 m. The supply air had a temperature of 15.7 °C and a relative humidity of 60%. In addition, the wheat bulk was subjected to self-weight and lateral pressure from the silo wall, leading to a non-uniform distribution of porosity inside the grain bulk. The

non-uniform porosity distribution formula of wheat bulk in this study is expressed as Equation (11) [20], and the porosity distribution cloud map is shown in Figure 2b.

$$\varepsilon = \varepsilon_0 - (\varepsilon_0 - \varepsilon_{\min}) \cdot (1 + 0.016H_b + 0.002t - 1.013) \quad (11)$$

where H_b is the depth of the grain unit, ε_0 is the initial porosity, $\varepsilon_{\min}$ is the minimum porosity inside the wheat bulk, which can be considered the porosity of the bottom surface of the grain bulk, and t is the storage time of the wheat.

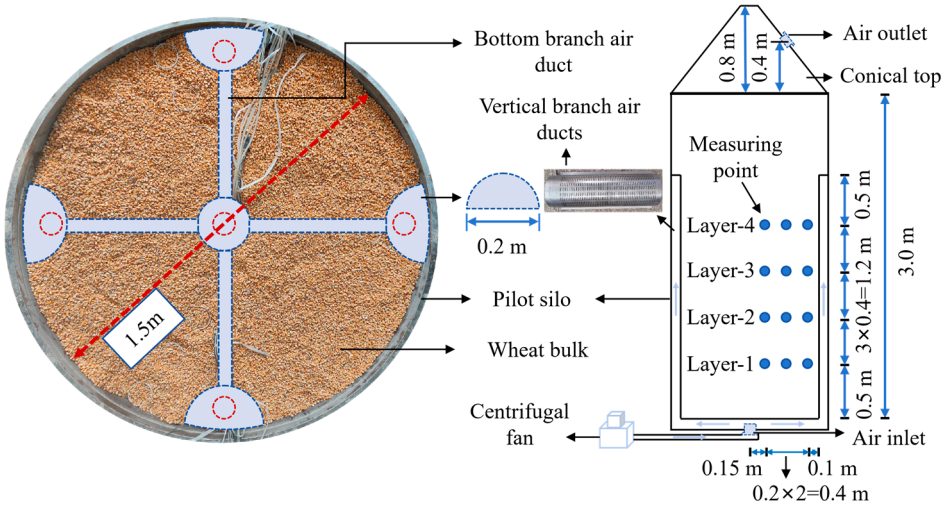

Figure 1. Pilot silo ventilation system.

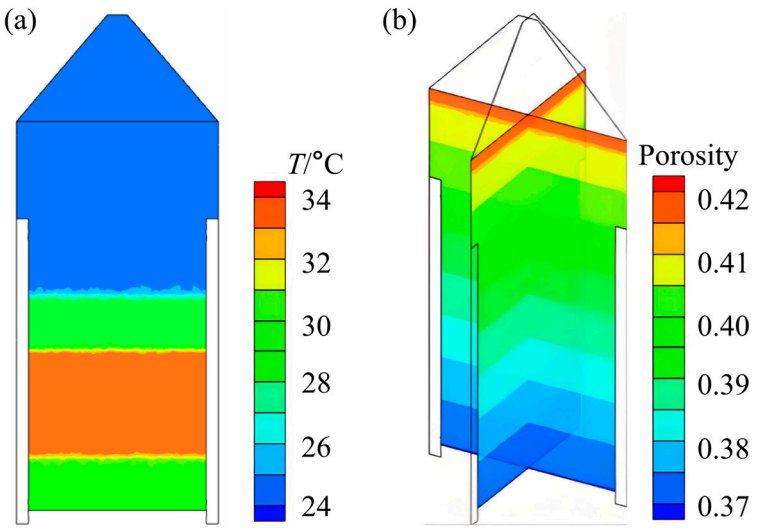

Figure 2. Model initialization parameter settings. (**a**) Temperature distribution. (**b**) Porosity distribution.

2.4. Sensitivity Analysis of the Ventilation Schemes

To investigate the influence of duct layout on ventilation performance under identical air supply conditions, the number of vertical branch ducts was varied and a central air collecting duct with a diameter of 0.2m was additionally incorporated. The cooling effects corresponding to different branch duct quantities and collecting duct heights were compared and analyzed. The numerical comparison schemes are presented in Figure 3 and Table 2. Specifically, the numbers of vertical branch ducts were set to 4, 6, and 8, evenly spaced along the silo wall; the heights of the central collecting duct were set to 0.47H, 0.94H, and 1.07H, where H represents the grain filling height. All listed cases share the same inlet boundary

condition, the same pressure outlet condition, and the same adiabatic wall treatment. These five cases compare branch duct number at a central duct height of 0.94H and central duct height with four branch ducts.

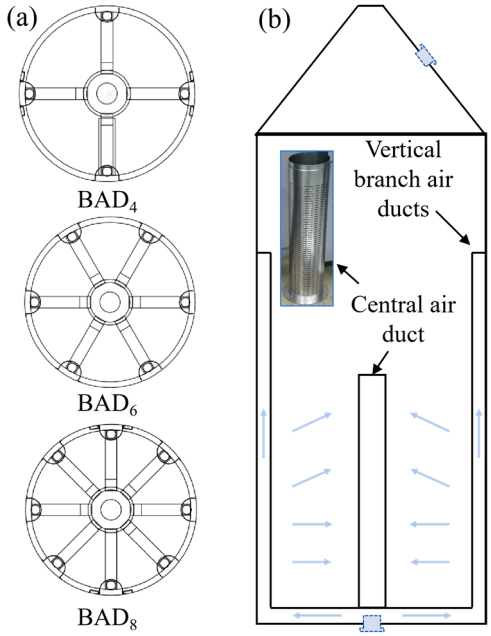

Figure 3. Arrangement scheme of vertical branch air ducts and central air duct: (**a**) vertical branch air ducts; (**b**) central air duct.

Table 2. Numerical simulation operating conditions.

	Height of Central Air Duct	Number of Vertical Branch Air Ducts
$BAD_{4–0.94}$	0.94H	4
$BAD_{6–0.94}$	0.94H	6
$BAD_{8–0.94}$	0.94H	8
$BAD_{4–0.47}$	0.47H	4
$BAD_{4–1.07}$	1.07H	4

2.5. Grid Model and Parameter Settings

The simulations were run with the commercial CFD package ANSYS Fluent (version 2019, ANSYS Inc., Canonsburg, PA, USA). The CFD geometry reproduced the actual dimensions of the pilot silo; it did not represent a full-size commercial silo. After the geometric model of the silo was optimized, a tetrahedral meshing scheme was used. Three sets of meshes were generated, with Mesh 1 consisting of 680,000 cells, Mesh 2 of 850,000 cells, and Mesh 3 of 980,000 cells. The inlet of the numerical model was specified as a mass flow inlet with a mass flow rate of 0.51 kg/s, while the outlet was set as a pressure outlet. Considering both simulation accuracy and computational time, the convergence residuals for the continuity, momentum, and moisture transport equations were set to 1.0×10^{-3}, and those for the energy equation were set to 1.0×10^{-6}. The SIMPLEC algorithm was adopted for pressure-velocity coupling. The under-relaxation factors for the energy and user-defined scalar (UDS) equations were both set to 0.8, and the temporal discretization scheme was set to first-order implicit. In addition, the viscous and inertial drag coefficients were calculated using the Ergun equation [19], yielding values of 2.21×10^{7} m^{-2} and 1.15×10^{3} m^{-1}, respectively. The initial temperature of the wheat bulk was assumed to be equal to that of the interstitial air. Cold air was supplied into the wheat bulk through a ventilation cage,

and the cold air entering the bulk exchanged heat with the grain, thereby achieving the cooling effect.

3. Results and Analysis

3.1. Verification of Numerical Simulation Method

To assess the temperature prediction capability of the numerical simulation method, the simulated temperatures of the wheat bulk with non-uniform porosity were compared with experimental measurements. First, the simulation results obtained with different mesh numbers were compared with the experimental data. Figure 4 presents a comparison between the experimental and simulated mean temperatures of each layer and the overall bulk during 88 h of mechanical ventilation. The numerical simulation results are in good agreement with the experimental measurements.

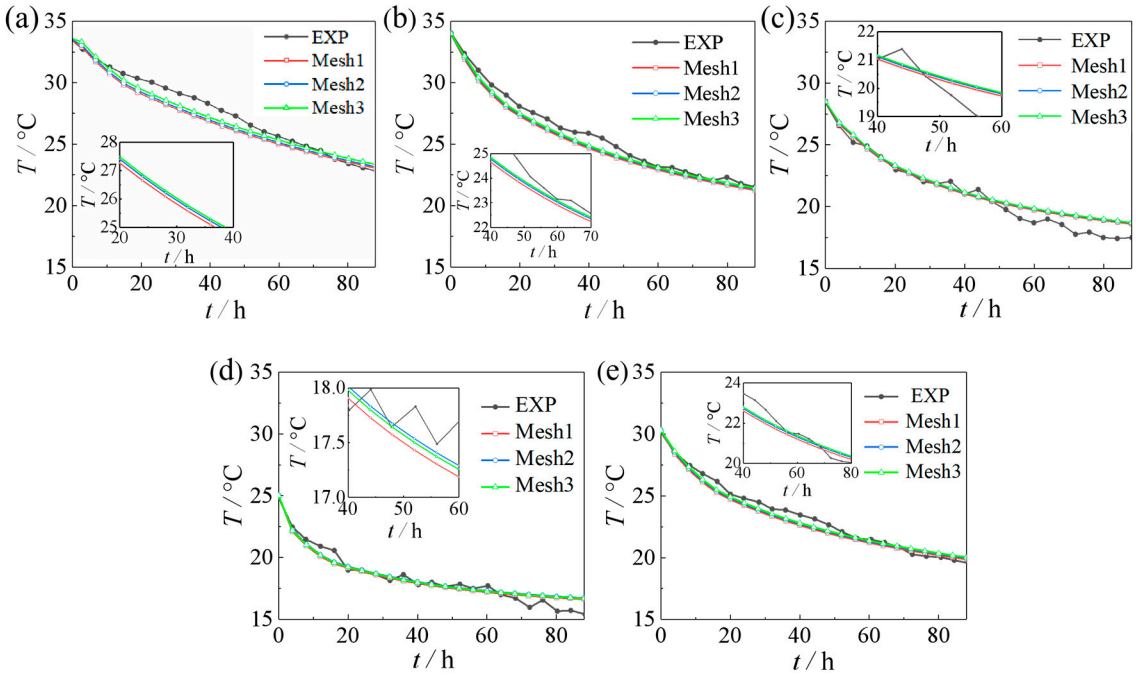

Figure 4. Comparison between experimental and simulated mean temperatures of different layers of the wheat bulk: (**a**) Layer-1, (**b**) Layer-2, (**c**) Layer-3, (**d**) Layer-4, (**e**) and Whole grain bulk.

Figure 4a–d show the comparison between the simulated mean temperatures of Layers 1 to 4 and the corresponding experimental temperatures during the 88 h mechanical ventilation process. The experimental results and the three sets of mesh-based simulations exhibited consistent trends overall. However, compared with the experimental data, the simulation results showed a slightly faster cooling rate. For Layers 1 and 2, the differences between the simulated and experimental values were relatively small during the initial 10 h and the final stage (from 60 h to the end), whereas a relatively large discrepancy was observed during the intermediate period (10–60 h). For Layers 3 and 4, the simulation results agreed well with the experimental data during the first 60 h; however, from 60 h onward, a notable deviation appeared between the simulated temperatures and the measured values. This deviation may be attributed to the influence of environmental factors, silo structural characteristics, and the internal air duct layout, which could not be maintained under stable conditions during the experiment, thereby leading to considerable errors between the experimental and simulated values for each layer at this stage. According to the experimental measurements, the initial temperatures of the different layers in the simulation varied, and

the supply air temperature did not reach a steady state over the ventilation period, resulting in different final temperatures for each layer.

Figure 4e shows the comparison between the overall mean temperature of the grain bulk during the 88 h ventilation process and the corresponding experimental reference. The simulation results from the three mesh schemes were consistent with the measured overall temperature trend, supporting the temperature prediction capability of the method for this pilot case. In addition, no significant differences were observed among the mean temperature results obtained from the three mesh schemes. Considering both accuracy and computational efficiency, the Mesh 1 scheme, which has a relatively smaller number of cells, was adopted for the subsequent CFD simulations.

3.2. The Influence of Different Numbers of Vertical Branch Air Ducts

To investigate the influence of the number of vertical branch air ducts on ventilation performance, three configurations with different branch duct quantities were examined, i.e., $BAD_{4–0.94}$, $BAD_{6–0.94}$ and $BAD_{8–0.94}$. The total inlet mass flow rate was kept constant at 0.51 kg/s in all cases, with the central duct height fixed at 0.94H. Consequently, increasing the number of vertical branch ducts decreased the flow rate per duct. The differences in cooling performance reported below therefore reflect the combined effects of the duct number (geometric effect) and the reduced flow rate per duct (hydraulic effect), rather than the geometric effect alone.

Figure 5 presents the streamline patterns and velocity distribution contours for the three branch duct configurations. The velocity distributions and streamline structures were generally similar across the three cases. The external airflow entered the perforated ventilation cage installed on the inner wall of the silo through the supply duct. Inside the ventilation cage, the airflow split into two paths: one part continued to flow upward along the height of the cage until reaching the closed top, where it then entered the grain bulk; the other part exited radially upward through the openings on the cage surface and penetrated into the surrounding grain bulk. In the upper region of the grain bulk, the airflow moved vertically along the silo height and was eventually discharged through the outlet at the top of the silo. In the lower region, below the top of the ventilation duct, the airflow entered the central air collecting duct and was conveyed upward and discharged through it.

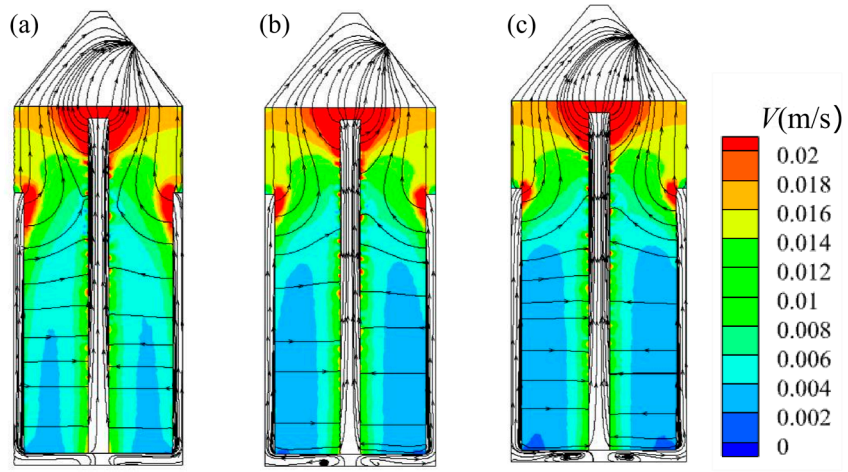

Figure 5. Streamline and velocity distribution contours for different branch duct configurations: (**a**) $BAD_{4–0.94}$, (**b**) $BAD_{6–0.94}$, and (**c**) $BAD_{8–0.94}$.

As the number of vertical branch ducts increased, a localized backflow phenomenon was observed near the inlet of the ventilation duct. Concurrently, the low-velocity zone

at the bottom of the grain bulk gradually expanded, whereas the high-velocity zone near the top of the vertical ducts within the grain bulk progressively shrank. Among the three configurations, the case with four vertical branch ducts exhibited a slightly faster initial cooling, although the differences among the three cases became small after about 40–88 h.

Figure 6 presents the mean temperature comparison for Layers 1 to 4 of the wheat bulk under different branch duct configurations during the 88 h ventilation process. During storage, temperatures below 20 °C can inhibit fungal growth and reduce grain spoilage; therefore, regions with temperatures above 20 °C can be regarded as high-temperature zones [21]. As the number of vertical branch ducts varied, a temperature difference among the three configurations was observed during the first 40 h, with $BAD_{4–0.94}$ exhibiting the most rapid decrease in temperature. After 40 h, the temperatures tended to converge across the three cases. This can be attributed to the combined geometric and hydraulic effects: as the number of branch ducts increased, the average airflow rate per duct decreased, resulting in a slower initial cooling rate. The individual contributions of duct geometry and flow rate distribution should be further distinguished in future work.

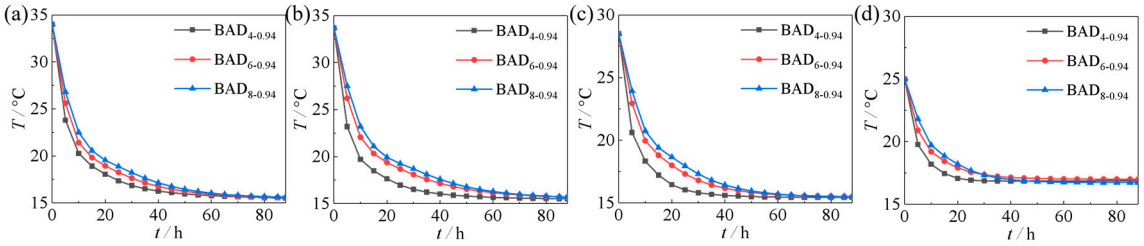

Figure 6. Temperature comparison of wheat bulk with different branch air ducts: (**a**) Layer-1, (**b**) Layer-2, (**c**) Layer-3, and (**d**) Layer-4.

Figure 7 presents the temperature distribution inside the wheat bulk after 24 h, 48 h, and 88 h of continuous ventilation for configurations with 4, 6, and 8 vertical branch ducts. At 24 h, the maximum temperatures within the wheat bulk were 28.5 °C, 28.7 °C, and 28.8 °C for the three configurations, respectively. After the low-temperature air entered the grain bulk, a cold front formed; however, a high-temperature zone emerged near the middle-to-lower region of the central air collecting duct, and the extent of this zone expanded as the number of branch ducts increased. This was attributed to the fact that the low-velocity zone at the bottom of the grain bulk enlarged with an increasing number of ducts, which hindered effective cooling of the grain bulk. At 48 h, the maximum temperatures decreased to 27.4 °C, 27.7 °C, and 27.9 °C, respectively, while the cold-front region expanded. The high-temperature zone near the middle-to-lower portion of the central air collecting duct disappeared, and the overall temperature declined. At 88 h, the maximum temperatures further decreased to 26.0 °C, 26.4 °C, and 26.6 °C, and the cold-front area continued to expand. The temperatures in most regions tended to become uniform, with the residual high-temperature zones mainly concentrated at the terminal end of the air duct, which was attributable to the so-called "short-circuit effect." At the end of the central air collecting duct, the airflow encountered greater resistance, making it preferentially pass through zones of lower resistance. While this effect intensified with an increasing number of ducts, the overall temperature distribution across the three configurations remained generally consistent.

Figure 8 presents the predicted changes in mean moisture content of the wheat bulk during 88 h of ventilation. Under all three operating conditions, the mean moisture content decreased rapidly during the first 20 h, accompanied by substantial evaporation and dissipation of moisture. After 20 h of ventilation, the moisture content tended to stabilize, with mean values of approximately 0.1225 (dry basis) for all three configurations. However, for the configuration with four vertical ducts, the mean moisture content was slightly higher

than that predicted for the six- and eight-duct cases, with a difference of about 0.0003 d.b. Among the three configurations, $BAD_{4–0.94}$ exhibited the fastest temperature decrease during the initial ventilation period (as shown in Figure 6), although the temperatures across the different configurations gradually converged over time. Notably, after ventilation, the temperature in the lower region of the grain bulk for $BAD_{4–0.94}$ was lower than that for $BAD_{6\text{-}0.94}$ and $BAD_{8–0.94}$. This lower-temperature zone created a relatively stable humidity environment, which slowed the evaporation rate of moisture and consequently resulted in a comparatively higher moisture content. Under the present fixed-flow conditions, $BAD_{4–0.94}$ provided slightly faster early-stage cooling and marginally higher predicted moisture retention, although the long-term differences among the three configurations were small. This ranking is restricted to the tested branch duct arrangements at a central duct height of 0.94H.

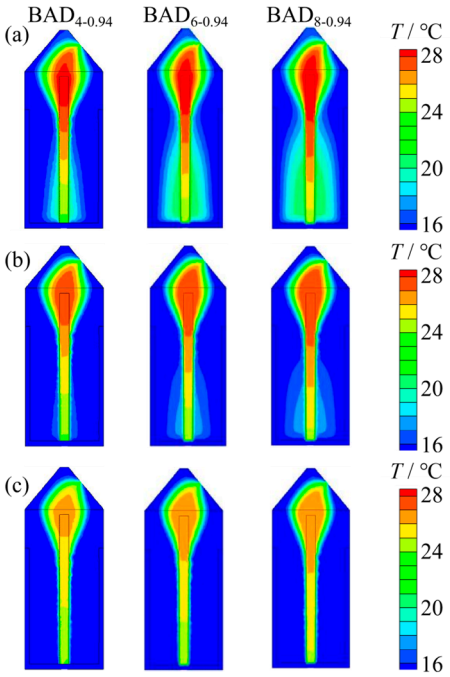

Figure 7. Temperature distribution contours for different numbers of vertical branch ducts at (**a**) 24 h, (**b**) 48 h, and (**c**) 88 h.

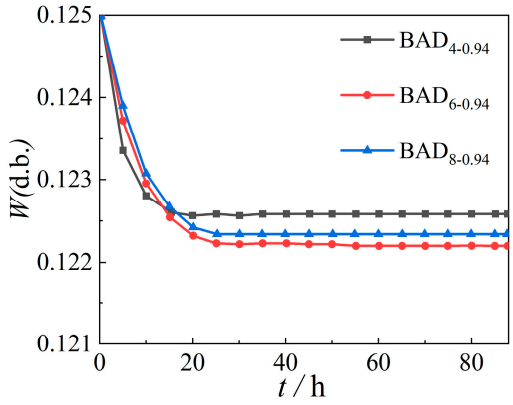

Figure 8. Comparison of mean moisture content of wheat bulk under different branch duct configurations.

Figure 9 presents the distribution of moisture content (dry basis) inside the wheat bulk after 24 h, 48 h, and 88 h of continuous ventilation for configurations with 4, 6, and

8 vertical branch ducts. At 24 h, the moisture content in the terminal region of the central air collecting duct was the lowest, at 9.6%, which corresponded to the high-temperature zone observed in that area. The moisture content in the lower portion of the grain layer exhibited considerable spatial variation, particularly in the vicinity of the central air collecting duct. At 48 h, the overall moisture content decreased slightly, and the low-moisture region at the tail of the central duct expanded. By 88 h, the moisture content in other regions of the grain bulk had gradually stabilized, and the moisture distribution became generally consistent across the three configurations. The observed trends in moisture content variation were in good agreement with the temperature changes described earlier. Considering both the cooling effect and moisture retention during the ventilation process, the $BAD_{4–0.94}$ configuration demonstrated superior overall control performance.

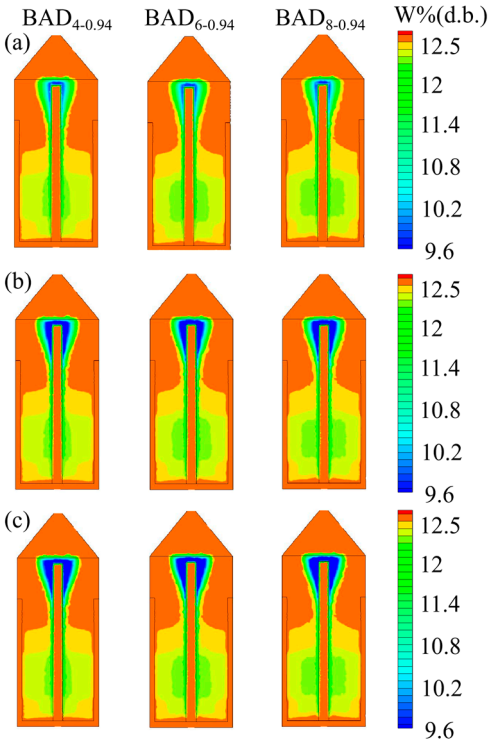

Figure 9. Distribution of moisture content inside wheat bulk after 24 h, 48 h, and 88 h of continuous ventilation under different branch duct configurations: (**a**) 24 h, (**b**) 48 h, and (**c**) 88 h.

3.3. Effects of Different Heights of Central Air Ducts

Based on the above findings, further investigations were conducted to examine the effect of central air collecting duct height on ventilation performance under the configuration with four branch ducts. Three duct height levels were considered: below the grain surface (0.47H), near the grain surface (0.94H), and above the grain surface (1.07H), as illustrated in Figure 10.

Figure 10 presents the streamline patterns and velocity distribution contours inside the wheat bulk for central air duct heights of 0.47H, 0.94H, and 1.07H. As illustrated, the external airflow entered the silo through the supply duct on the inner wall and penetrated into the grain layer. Part of the airflow passed directly through the grain layer and was discharged from the outlet at the top of the silo, while the remainder entered the central air collecting duct through the grain layer and was also exhausted from the top outlet along the duct. The primary distinction among the configurations lay in the airflow path length: for the case with a central duct height of 0.47H, the airflow traversed a longer path through

the grain bulk, passing vertically through the upper grain layer before being discharged from the top.

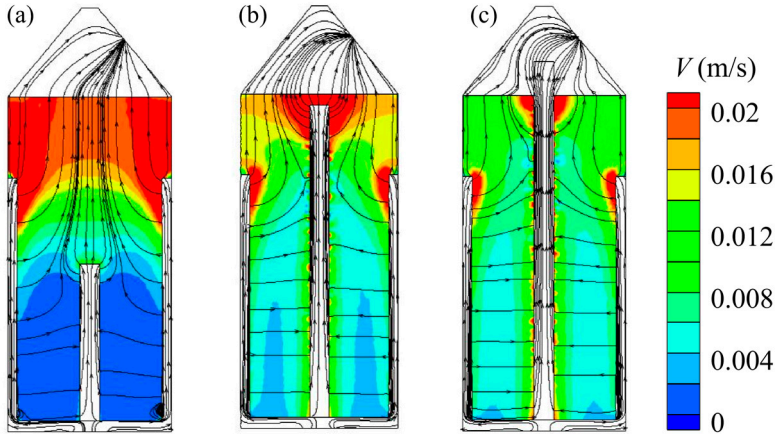

Figure 10. Streamline and velocity distribution contours at different central duct heights: (**a**) $BAD_{4–0.47}$, (**b**) $BAD_{4–0.94}$ and (**c**) $BAD_{4–1.07}$.

The airflow velocity in the middle and lower regions of the grain bulk decreased as the central duct height increased. This can be attributed to the relatively low porosity in these regions, which imposed higher resistance to airflow, thereby favoring discharge through the central air collecting duct. Moreover, a greater duct height was associated with improved ventilation performance. In the $BAD_{4–0.47}$ configuration, the absence of a central air collecting duct in the upper portion of the grain bulk forced the airflow to pass solely through the grain layer, resulting in a large high-velocity zone. In contrast, the $BAD_{4–0.94}$ and $BAD_{4–1.07}$ configurations exhibited only a small high-velocity region near the terminal end of the central duct, owing to the presence of the central air collecting duct.

Figure 11 presents the comparison of mean temperatures for Layers 1 to 4 of the wheat bulk during the 88 h ventilation process under different central air duct heights. The temperature distribution within the grain bulk was notably influenced by the central duct height, especially during the early and intermediate stages. When the duct height was increased from 0.47H to 0.94H, the mean temperatures of Layers 1 to 3 exhibited significant reductions, with Layer 1 showing the largest decrease of 4.63 °C. When the duct height was further increased from 0.94H to 1.07H, the mean temperatures of all four layers decreased, with Layer 4 demonstrating the most pronounced reduction. These improvements can be attributed to the fact that as the central duct height increased, the airflow path was optimized, thereby reducing the residence time of air within the grain layer.

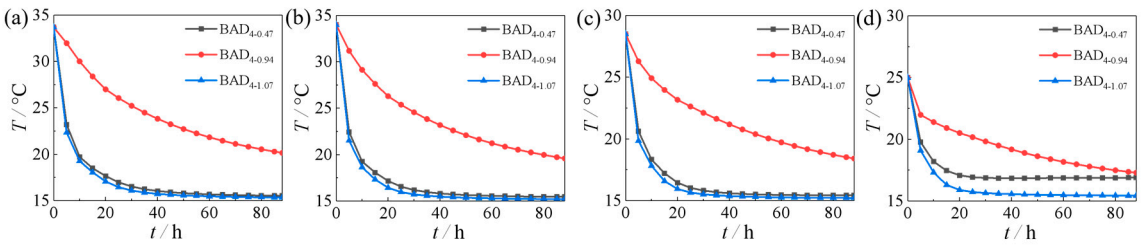

Figure 11. Comparison of mean temperatures for different grain layers under various central duct heights: (**a**) Layer-1, (**b**) Layer-2, (**c**) Layer-3, and (**d**) Layer-4.

Figure 12 presents the temperature distribution inside the wheat bulk during continuous ventilation for 24 h, 48 h, and 88 h at central air duct heights of 0.47H, 0.94H, and 1.07H. At 24 h, the maximum temperatures in the wheat bulk were 30.0 °C, 28.5 °C, and 26.4 °C

for the three configurations, respectively. At 24 h, the maximum temperature decreased as the tested central duct height increased, consistent with changes in airflow discharge paths. At later times, the maximum-temperature ranking was not monotonic with duct height, as the values below show. The maximum high-temperature zone area ratio for $BAD_{4–0.47}$ was 0.449 (Figure 13). At 48 h, the maximum temperatures were 25.6 °C, 27.4 °C, and 24.8 °C, respectively. Prolonging the ventilation time enlarged the cold-front region, reduced the extent of the high-temperature zone, and led to an overall decline in the grain bulk temperature. At 88 h, the maximum temperatures decreased to 23.5 °C, 26.0 °C, and 22.1 °C, respectively. The temperature continued to decrease, and the high-temperature zone area ratios for $BAD_{4–0.47}$ and $BAD_{4–1.07}$ were 0.092 and 0.047, respectively, which were relatively small. However, for $BAD_{4–0.94}$, a high-temperature zone area ratio of 0.159 remained in the terminal region of the central air duct. This was attributed to the fact that the resistance to airflow through the ventilation duct toward the grain surface was lower than that through the central air duct, causing the airflow to preferentially flow toward the path of lower resistance. Over the simulated ventilation interval, the high-temperature-zone area ratio for each configuration was described by the empirical exponential fit in Equation (12):

$$\frac{A_{high}}{A_{total}} = (1 - y_0)e^{-t/a} + y_0 \tag{12}$$

where A_{high}/A_{total} is the high-temperature area ratio of wheat bulk; t is the ventilation time; a, y_0 are empirical fitting parameters for the individual configurations and simulated ventilation interval; and the specific parameters are shown in Table 3. These fits summarize the present simulations and should not be extrapolated to other geometries, inlet conditions, or ventilation durations without further assessment.

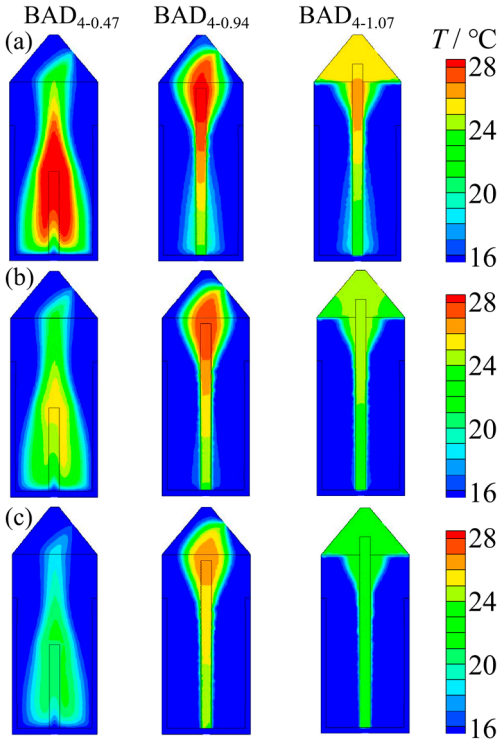

Figure 12. Temperature distribution contours inside the wheat bulk under different central air duct heights after 24 h, 48 h, and 88 h of continuous ventilation: (**a**) 24 h, (**b**) 48 h, and (**c**) 88 h.

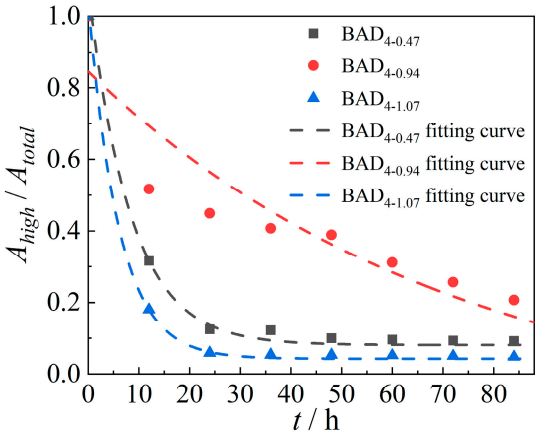

Figure 13. Area ratio of high-temperature zones in wheat bulk under different central air duct heights.

Table 3. Table of fitting parameters.

	a	y_0	R^2
$BAD_{4–0.47}$	8.299	0.081	0.988
$BAD_{4–0.94}$	72.787	−0.155	0.843
$BAD_{4–1.07}$	6.046	0.042	0.997

Figure 14 presents the predicted changes in mean moisture content of the wheat bulk during 88 h of ventilation under different central air duct heights. The moisture content tended to stabilize, with $BAD_{4–0.94}$ at approximately 0.1225 and $BAD_{4–1.07}$ at around 0.123, which can be attributed to the rapid temperature decrease during the early stage of ventilation. The predicted final moisture content did not decrease monotonically with duct height: $BAD_{4–0.94}$ had a lower value than $BAD_{4–1.07}$, while $BAD_{4–0.47}$ retained the most moisture. Thus, the configuration with the smallest residual high temperature zone area was not the one with the greatest moisture retention. The decreasing rate of moisture content for $BAD_{4–0.47}$ was relatively slow, which corresponded well with its temperature variation. $BAD_{4–0.47}$ had the highest predicted mean moisture content among the three height configurations, approximately 0.1235 after 88 h.

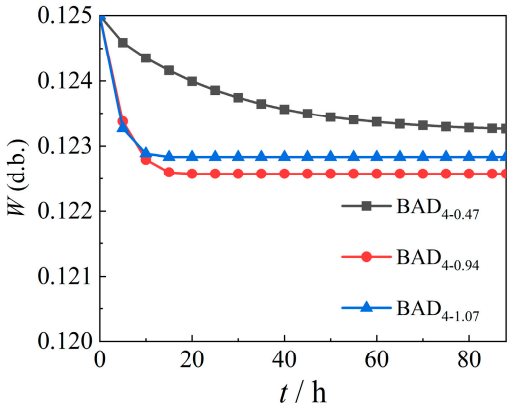

Figure 14. Comparison of the mean moisture content of the wheat bulk under different central air duct heights.

Figure 15 presents the distribution of moisture content (dry basis) inside the wheat bulk under continuous ventilation for 24 h, 48 h, and 88 h at central air duct heights of 0.47H, 0.94H, and 1.07H. At 24 h, little change was observed in the moisture distribution for

$BAD_{4–0.47}$, whereas the lower regions of $BAD_{4–0.94}$ and $BAD_{4–1.07}$ exhibited notable variations, with a low-moisture zone appearing at the terminal end of the central air duct, particularly for the 0.47H configuration. This observation corresponded to the high-temperature region at the tail of the central duct shown in Figure 12. After 48 h, the overall moisture content decreased slightly, especially at the terminal end of the central duct where airflow was relatively strong. By 88 h, the extent of the low-moisture zone at the central duct end had expanded, while the overall moisture distribution tended to stabilize. Owing to the reduced moisture content of the grain bulk and the sustained ventilating and cooling environment, the rate of moisture decrease gradually slowed down.

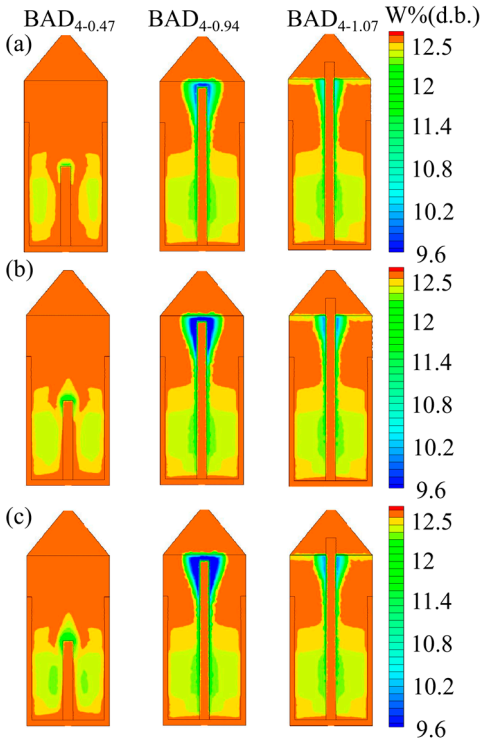

Figure 15. Distribution of moisture content inside wheat bulk under different central air duct heights after 24 h, 48 h, and 88 h of continuous ventilation: (**a**) 24 h, (**b**) 48 h, and (**c**) 88 h.

3.4. Engineering Implications and Limitations

This simulation study demonstrates how airflow redistribution in a non-uniform porous body can leave residual warm zones near duct ends and why volume-averaged temperature alone may not adequately describe spatial cooling performance. It also shows that the configuration producing the smallest residual hot-zone area does not necessarily produce the smallest moisture loss. These considerations may be useful when evaluating other grain aeration systems, but the present calculations do not determine their scale or specific configuration in such systems. The quantitative results of this study are limited to the wheat volume, porosity distribution, pilot-scale silo geometry, and duct layout investigated. The reported temperature differences, humidity values, hot-zone area ratios, exponential fitting parameters, and preferred configurations require further validation before being transferred to commercial silos or other operating conditions.

Future work should use sampling that minimally disturbs the grain bulk to validate moisture predictions and should evaluate full-scale silos, other grain materials, and variable inlet temperature, humidity, and airflow rates. A wider range of duct heights, as well as combinations of duct number and height, is needed to evaluate configuration interactions.

Before optimization or control methods are used to formulate design recommendations, comparing constant flow per duct would help separate geometric and hydraulic effects.

4. Conclusions

This study applied an established coupled heat and moisture transfer framework to compare radial ventilation duct configurations in a pilot-scale wheat silo with non-uniform porosity. Its contribution is the configuration-specific interpretation of airflow, cooling, and predicted moisture responses. The main conclusions are summarized as follows:

1. A coupled heat and moisture transfer model accounting for non-uniform porosity distribution was implemented using standard porous media transport equations, the Ergun equation, and a thin-layer drying model. The model reproduced the measured temperature evolution of the wheat bulk in this pilot silo with good agreement.

2. At a total inlet mass flow rate of 0.51 kg/s and a central duct height of 0.94H, the four-, six-, and eight-branch duct cases differed mainly in early cooling and predicted moisture variation. Four branch ducts gave slightly faster initial cooling and marginally higher predicted moisture retention, while differences diminished during approximately 40–88 h.

3. The height of the central air collecting duct affected both the location and extent of high-temperature zones within the wheat bulk. The area of the high-temperature zone decreased exponentially with ventilation time. Among the three tested central-duct heights in this pilot silo, 1.07H gave the most rapid reduction in the high-temperature zone, whereas 0.94H gave the lowest final moisture content. A central air collecting duct positioned near or above the grain surface is beneficial for regulating the ventilation performance of the grain bulk, but the preferred height depends on whether rapid cooling or moisture retention is the primary objective.

The broader engineering implication is to assess airflow distribution, residual warm regions, and moisture retention together when comparing grain aeration layouts. The numerical values and configuration rankings remain specific to the investigated wheat bulk, pilot geometry, porosity profile, and operating conditions; extension to other systems requires further validation.

Author Contributions: Conceptualization, H.S. and G.Z.; methodology, H.S. and G.Z.; software, D.Z. and S.Y.; validation, Z.Y.; formal analysis, D.Z. and C.L.; investigation, Z.Y. and S.Y.; resources, G.Z. and Z.Y.; data curation, C.L. and S.Y.; writing—original draft preparation, H.S. and C.L.; writing—review and editing, D.Z.; supervision, G.Z. and D.Z.; project administration, G.Z. and D.Z.; funding acquisition, D.Z. and C.L. All authors have read and agreed to the published version of the manuscript.

Funding: This research was funded by the National Natural Science Foundation of China (NSFC) project (grant number 52676061); Henan Provincial Natural Science Foundation Project (grant number 252300423559); Henan Province Science and Technology R&D Program Joint Fund (grant number 252301420043 and 252301420055); the Scientific and Technological Project of Henan Province (grant number 252102110345); Wuxi COFCO Engineering Technology Co., Ltd. Technical Service Project (grant number WXGKZY2026006-001); the Key R&D projects in Henan Province (grant number 241111322600).

Institutional Review Board Statement: Not applicable.

Informed Consent Statement: Not applicable.

Data Availability Statement: The original contributions presented in this study are included in the article. Further inquiries can be directed to the corresponding author(s).

Conflicts of Interest: Authors Huichen Shi, Gang Zhang, and Zhipeng Yao were employed by the company Wuxi COFCO Engineering & Technology Co., Ltd. The remaining authors declare that the research was conducted in the absence of any commercial or financial relationships that could be construed as a potential conflict of interest.

References

1. National Bureau of Statistics. *China Statistical Yearbook*; China Statistics Press: Beijing, China, 2020. Available online: https://www.stats.gov.cn/sj/ndsj/2025/indexch.htm (accessed on 15 July 2026).
2. Dorosh, P.; Minot., N.; Rashid, S. Food price stabilization: Theory and lessons from experience. *Food Policy* **2025**, *137*, 102945. [CrossRef]
3. Salarikia, A.; Jian, F.J.; Jayas, D.S.; Zhang, Q. Segregation of dockage and foreign materials in wheat during loading into a 10-m diameter corrugated steel bin. *J. Stored Prod. Res.* **2021**, *93*, 101837. [CrossRef]
4. Cheng, X.D.; Zhang, Q.; Shi, C.X.; Yan, X.J. Model for the prediction of grain density and pressure distribution in hopper-bottom silos. *Biosyst. Eng.* **2017**, *163*, 159–166. [CrossRef]
5. Ziegler, V.; Paraginski, R.; Ferreira, C. Grain storage systems and effects of moisture, temperature and time on grain quality-a review. *J. Stored Prod. Res.* **2021**, *91*, 101770. [CrossRef]
6. Zhu, Y.H.; Li, H.; Zhen, T.; Li, Z.H. Integrating self-attention mechanisms and ResNet for grain storage ventilation decision making: A study. *Appl. Sci.* **2023**, *13*, 7655. [CrossRef]
7. Lawrence, J.; Maier, D.E. Prediction of temperature distributions in peaked, leveled and inverted cone grain mass configurations during aeration of corn. *Appl. Eng. Agric.* **2012**, *28*, 685–692. [CrossRef]
8. Li, X.; Wang, Y.C.; Yang, K.M.; Du, X.M. Numerical study of heat and mass transfer during drying process of barley grain piles based on the pore scale. *J. Food Process Eng.* **2023**, *46*, e14433. [CrossRef]
9. Gao, M.Y.; Cheng, X.D.; Du, X.C. Simulation of bulk density distribution of wheat in silos by finite element analysis. *J. Stored Prod. Res.* **2018**, *77*, 1–8. [CrossRef]
10. Moya, M.; Aguado, P.J.; Ayuga, F. Mechanical properties of some granular agricultural materials used in silo design. *Int. Agrophysics* **2013**, *27*, 181–193. [CrossRef]
11. Panigrahi, S.S.; Singh, C.B.; Fielke, J. CFD modelling of physical velocity and anisotropic resistance components in a peaked stored grain with aeration ducting systems. *Comput. Electron. Agr.* **2020**, *179*, 105820. [CrossRef]
12. Khatchatourian, O.; Savicki, D. Mathematical modelling of airflow in an aerated soya bean store under non-uniform conditions. *Biosyst. Eng.* **2004**, *88*, 201–211. [CrossRef]
13. Jian, F.; Jayas, D.S.; White, N.D. Temperature fluctuations and moisture migration in wheat stored for 15 months in a metal silo in Canada. *J. Stored Prod. Res.* **2009**, *45*, 82–90. [CrossRef]
14. Nwaizu, C.; Zhang, Q. Computational modeling of heterogenous pore structure and airflow distribution in grain aeration system. *Comput. Electron. Agric.* **2021**, *188*, 106315. [CrossRef]
15. Zheng, D.Q.; Li, L.; Chen, G.X.; Zhou, Y.; Liu, K. Numerical study of low-temperature ventilation drying in a wheat grain silo considering non-uniform porosity distribution. *Appl. Sci.* **2024**, *14*, 96. [CrossRef]
16. Yan, J.C.; An, J.Y.; Wei, H.; Xie, H.X.; Zhao; Q. You, Z.Y. Cooling and dehydration behavior of wet wheat using hexagonal air duct aeration. *Case Stud. Therm. Eng.* **2025**, *73*, 106425. [CrossRef]
17. Eisfeld, B.; Schnitzlein, K. A new pseudo-continuous model for the fluid flow in packed beds. *Chem. Eng. Sci.* **2005**, *60*, 4105–4117. [CrossRef]
18. Thorpe, G.R. The application of computational fluid dynamics codes to simulate heat and moisture transfer in stored grains. *J. Stored Prod. Res.* **2008**, *44*, 21–31. [CrossRef]
19. Ergun, S. Fluid flow through packed columns. *Chem. Eng. Prog.* **1952**, *48*, 89.
20. Ertekin, C.; Firat, M.Z. A comprehensive review of thin-layer drying models used in agricultural products. *Crit. Rev. Food Sci. Nutr.* **2017**, *57*, 701–717. [CrossRef]
21. Mohapatra, D.; Kumar, S.; Kotwaliwale, N.; Singh, K.K. Critical factors responsible for fungi growth in stored food grains and non-Chemical approaches for their control. *Ind. Crop. Prod.* **2017**, *108*, 162–182. [CrossRef]

Disclaimer/Publisher's Note: The statements, opinions and data contained in all publications are solely those of the individual author(s) and contributor(s) and not of MDPI and/or the editor(s). MDPI and/or the editor(s) disclaim responsibility for any injury to people or property resulting from any ideas, methods, instructions or products referred to in the content.